Impurity scattering in *p*-type silicon nanowire FET: *k.p* approach

N.D. Akhavan, G. Jolley, G. Umana-Membreno, J. Antoszewski, L. Faraone
Microelectronics Research Group, School of Electrical, Electronic and Computer Engineering,
The University of Western Australia, WA 6009
Email: nima.dehdashti@uwa.edu.au

***Abstract*— Influence of an acceptor impurity atom in the channel of *p*-type silicon nanowire in [100], [110] and [111] crystal orientations has been studied using a three-dimensional non-equilibrium Green's function formalism. The valence band has been modeled using a 6-band *k.p* Hamiltonian. At low gate bias, the drain current differs from homogenous channel due to resonance levels and screening of carries in the channel by ionized impurities, whereas at high gate bias, the drain current is dominated by the thermionic current. It is also shown that the impurity induced density of stated are profound in low energy subbands.**

I. INTRODUCTION

Despite numerous studies on quantum transport in *n*-type silicon nanowire FET in the past few years, hole transport in *p*-type silicon nanowire has been neglected due to the complex nature of valence bandstructure of silicon [1,2]. However, a recently developed theoretical approach based on the *k.p* description of valence bands and NEGF formalism has enabled modeling of the hole transport with high accuracy that is comparable to the tight-binding (TB) method with reasonable computational cost. Most of these studies have been limited to optimizing *k.p* parameters and comparing results with TB Hamiltonian [2-7]. Here, we show that solutions of the *k.p* Hamiltonian in mode-space can be effectively used to model valence band and scattering in the presence of ionized impurity atom in silicon nanowire FETs.

II. SIMULATION PROCEDURE

A. K.p theory

In order to model the hole transport in *p*-type silicon nanowire, we have followed the simulation approach outlined in [3,6]. The 6×6 *k.p* Hamiltonian for [100] crystal orientation can be written as [6]:

$$H_{k.p}=\begin{bmatrix} H_{3\times3} & \\ & H_{3\times3} \end{bmatrix}+\Delta_{SO}\begin{bmatrix} iG & \Gamma \\ -\Gamma^{*} & -iG \end{bmatrix} \tag{1}$$

where,

$$H_{3\times3}=\begin{bmatrix} Lk_x^2+M(k_y^2+k_z^2) & Nk_xk_y & Nk_xk_z \\ Nk_xk_y & Lk_y^2+M(k_x^2+k_z^2) & Nk_yk_z \\ Nk_xk_z & Nk_yk_z & Lk_z^2+M(k_x^2+k_y^2) \end{bmatrix} \tag{2}$$

is the Kane's 3×3 interaction matrix that contains the three parameters $L = \hbar\ (-\gamma_1 - 4\gamma_2)\ /\ 2m_0$, $M = \hbar\ (-\gamma_1 + 2\gamma_2)\ /\ 2m_0$ and $N = -6\hbar\ \gamma_3/\ 2m_0$, where γ_1 , γ_2 and γ_3 are the Lüttinger parameters, Δ_{SO} is the split-off parameter, and A and B are spin-orbit (SO) coupling matrices. Turning off the SO interaction, the second matrix in (1) will become zero and the total Hamiltonian is reduced to $H_{k.p}$=$H_{3\times3}$ with double degeneracy. In order to obtain $H_{k.p}$ for nanowire along [110] and [111] direction, one needs to rotate the $H_{k.p}$ and K vector using rotation matrix. The coordinate transformation matrix Ū is defined as [10, 11]:

$$\bar{U}(\theta,\varphi)=\begin{bmatrix} \cos\varphi\cos\theta & \sin\varphi\cos\theta & -\sin\theta \\ -\sin\varphi & \cos\varphi & 0 \\ \cos\varphi\sin\theta & \sin\varphi\sin\theta & \cos\theta \end{bmatrix} \tag{3}$$

where θ and φ are are the polar and azimuthal angles of the *z*-axis in the crystallographic coordinate system. Having built the transformation matrix for a desired crystal orientation, we can obtain the Hamiltonain and K vector in a new coordinate system as follows:

$$H'_{3\times3}=\bar{U}H_{3\times3}\bar{U}^{T} \tag{4}$$

$$\begin{bmatrix} k_x \\ k_y \\ k_z \end{bmatrix}=\bar{U}^{T}\begin{bmatrix} k'_x \\ k'_y \\ k'_z \end{bmatrix} \tag{5}$$

978-1-4673-5736-4/13/$31.00 ©2013 IEEE

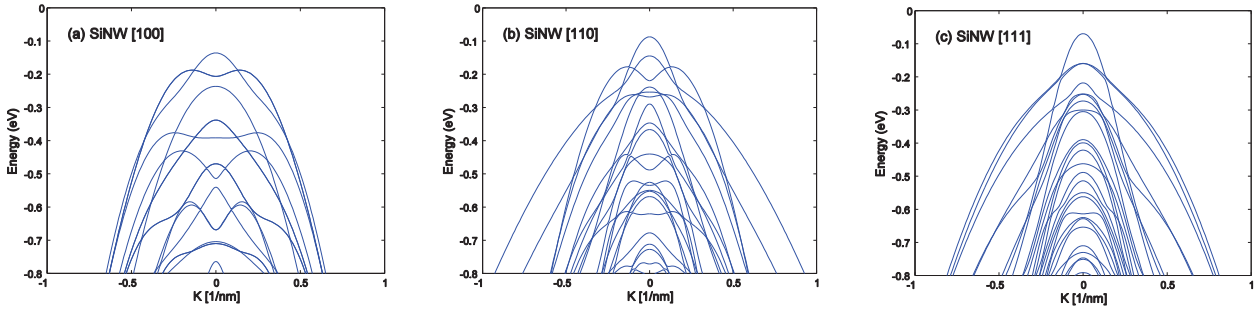

Fig. 1. Band structure of 5×5 nm^2 Si nanowire in [100], [110] and [111] crystal orientations with tuned lüttinger parameters and SO interactions turned off.

for nanowire oriented in [110] direction, θ=90 and φ=45 and for [111] we have $\tan^{-1}\theta = \sqrt{2}$ and φ=-45, rspectively. Fig. 1 shows the bandstructure for different crystal orientations by applying rotation matrix t0 [100] Hamiltonian. For numerical calculations, we first discretize the Hamiltonian of Eq. (1) in the real space by substituting $k_v = -i\partial/\partial_v$, where $v=x, y, z$. We then transform the discretized real-space Hamiltonian H_R to k-space Hamiltonian using the following relation [3]:

$$H_K = U_K^+ H_R U_K \tag{3}$$

where unitary matrix U_K is a block diagonal matrix and its diagonal blocks represents the two-dimensional sine transformation. The Hamiltonian in k-space can be further transformed to the mode-space via:

$$H_M = U_M^+ H_K U_M \tag{4}$$

where U_M is the transformation matrix which is constructed as follows. The "mode" wavefunction ψ_m is defined as the wavefunction at k=0 of the E-k diagram, where $1 \le m \le Nm$ and N_m is the number of the modes as shown in Fig. 2. We can then construct the unitary matrix U0 which consists of ψ_m as its column vectors:

$$U_0 = \left(|\psi_1\rangle |\psi_2\rangle \cdots |\psi_m\rangle \right) \tag{5}$$

for the i-th nanowire cross-section, U_M is calculated as follows:

$$U_M(i) = U_0 U_i \tag{6}$$

where U_i is the matrix which diagonalizes the following matrix:

$$h_i = \varepsilon_0 + U_0^+ V_i U_0 \tag{7}$$

where ε_0 is the energies at k=0 of the E-k diagram and V_i is the k-space, two dimensional potential profile of the i-th cross-section and is computed as follows:

$$V_K(i) = U_K^+ V_R(i) U_K \tag{8}$$

where $V_R(i)$ is the discretized real-space two-dimensional potential profile at i-th cross-section of the nanowire.

The transformed Hamiltonian in mode-space automatically considered the mode-coupling and hence it can be applied to nanowire with surface roughness where we have strong mode coupling.

Through successive transformation from real-space as outlined above, the effective size of Hamiltonian can be reduced considerably in mode-space. In this work we have considered a nanowire with 5×5 nm^2 cross-section, 10 nm channel length, source/drain extension of 10 nm and 1nm oxide thickness. For numerical simulations $N_y=N_z=50$, $N_x=200$ and $N_b=3$ where N_y,N_z and N_x are finite difference spacing in y, z, x direction and Nb is the number of bands in $k.p$ Hamiltonian. The finite difference method (FDM) discretization results in real-space Hamiltonian whose block diagonal elements are of size $N_y \times N_z \times N_b$ or 7500 which is too big for numerical simulation. This can be reduced to 600 and 200 for k-space and mode-space Hamiltonian.

B. NEGF simulation details

Having built the mode-space Hamiltonian by the strategy outlined above, we can employ the non-equilibrium Green's function (NEGF) formalism to compute charge and current density in the nanowire. NEGF approach is a well-established standard method to perform quantum transport in nanostructures [8]. The real-space hole density is obtained by:

$$\rho(r) = U_R \rho_M U_R^+ \tag{9}$$

where $U_R = U_K U_M$ is the matrix which transforms back the mode-space charge density to real-space charge density. Mode-space charge density is computed by:

$$\rho_M = \frac{1}{2\pi} \int \left(f_s G s \Gamma_s G_s^+ + f_d G_d \Gamma_d G_d^+ \right) dE \tag{10}$$

where $f_{s(d)}$ is the Fermi function at source (s) and drain (d) and $\Gamma_{s(d)}$ is the broadening function which is defined as:

$$\Gamma_{s(d)} = i\left(\Sigma_{s(d)} - \Sigma_{s(d)}^+ \right) \tag{11}$$

where $\Sigma_{s(d)}$ is the self-energy matrix at source/drain which can be computed by iterative methods such as Sancho-Robio algorithm or by boundary matrix eigenvalue problem[9-11]. Having solved the NEGF equations, calculated hole density is fed into the three-dimensional Poisson solver to update the potential profile as follows:

$$\nabla^2 \varphi^k = -\frac{q}{\varepsilon} \left(N_D + \rho^k e^{-(\varphi^k - \varphi^{k-1})/k_B T} \right) \tag{12}$$

where φ^k and ρ^k are the k-th self-consistent step solutions for potential and hole density. The 3D Poisson's equation has been solved by COMSOL® multyphyics solver which employs finite element method and energy integration in Equ. 2 has been computed by adoptive integration method.

III. Simulation Results

We have considered a nanowire in [100], [110] and [111] orientations with L_S=L_D=L_{ch}=10 nm and T_{ox}=1 nm. The channel region is intrinsic and source/drain extensions have doping density of 1e20 cm^{-3}. The impurity has been included by non-pertubative approach in the Poisson's equation which is modelled as a sphere with a radius of 0.2 nm. The charge density associated to this impurity can be written as: $N_{impurity}=1/V^3$, where V is the volume of sphere. The inpurity has been put in the middle of the channel and in center of the *yz*-plane prependicular to transport direction. Fig. 3. Shows the I_{DS}-V_{GS} curves for different crystal orientations. It is evident that [100] direction has the lowest current due to highest hole effective mass. Fig. 4 shows the I_{DS}-V_{GS} curve for nanowire with and without impurity. The impurity has highest influence on the drain current in subthreshold region. Fig. 5 and Fig. 6 show the 1st subband energy and 1D hole density along the nanowire in [100] direction for acceptor type impurity as a function of V_{GS}. Fig. 7 and Fig. 8 show the energy-resolve local density of states and hole density at V_{GS}=0.6 for nanowire in [100] direction. Unlike n-type nanowire the impurity induced LDOS are located are lower energy levels as shown in Fig. 9. Shows the 2D hole density at V_{GS}=0.9 V and V_{GS}=0.3 V [2,3].

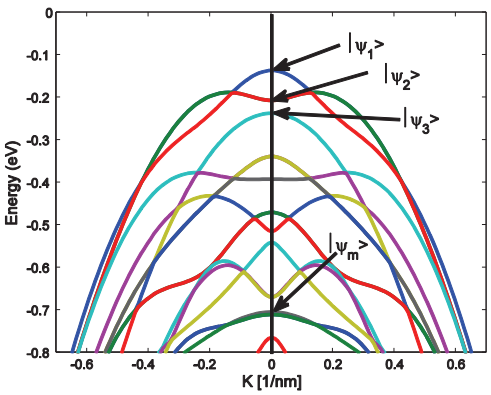

Fig. 2. Mode selection at k=0 in [100] Si nanowire.

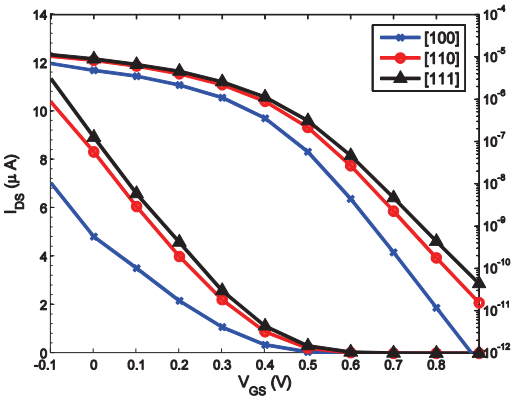

Fig. 3. I_{DS}-V_{GS} characteristic for different crystal orientations. Nanowire in [111] has the highest current density.

IV. Conclusion

We performed self-consistent simulations of impurity scattering in the *p*-type silicon nanowires using a 3-band *k.p* approach for different crystal orientations. We showed that the mode-space approach can reproduce results with much less computational resources than real-space while retaining the accuracy in a reasonable limit. This method can also be used to study different sources of variability (random dopant, surface roughness, etc.) in *p*-type silicon nanowire.

Acknowledgment

This work has been supported by the Australian Research Council under the Super Science Fellowship program grant number FS110200022.

References

[1] A. Martinez, N. Seoane, A. R. Brown *et al.*, "Variability in Si Nanowire MOSFETs Due to the Combined Effect of Interface Roughness and Random Dopants: A Fully Three-Dimensional NEGF Simulation Study," *Electron Devices, IEEE Transactions on,* vol. 57, no. 7, pp. 1626-1635, 2010.

[2] N. Dehdashti Akhavan, I. Ferain, R. Yu *et al.*, "Emission and absorption of optical phonons in Multigate Silicon Nanowire MOSFETs," *Journal of Computational Electronics,* vol. 11, no. 3, pp. 249-265, 2012.

[3] N. D. Akhavan, I. Ferain, R. Yu et al., "Influence of discrete dopant on quantum transport in silicon nanowire transistors," Solid-State Electronics, vol. 70, no. 0, pp. 92-100, 2012.

[4] M. Shin, "Full-quantum simulation of hole transport and band-to-band tunneling in nanowires using the k.p method," Journal of Applied Physics, vol. 106, no. 5, pp. 054505-054505-10, 2009.

[5] M. Shin, "Effect of channel orientation in p-type nanowire Schottky barrier metal-oxide-semiconductor field-effect transistors," Applied Physics Letters, vol. 97, no. 9, pp. 092108-092108-3, 2010.

[6] M. Shin, L. Sunhee, and G. Klimeck, "K.p-based quantum transport simulation of silicon nanowire pMOSFETs," in Nanotechnology, 2009. IEEE-NANO 2009. 9th IEEE Conference on, 2009, pp. 374-377.

[7] M. Shin, L. Sunhee, and G. Klimeck, "Computational Study on the Performance of Si Nanowire pMOSFETs Based on the k.p Method," Electron Devices, IEEE Transactions on, vol. 57, no. 9, pp. 2274-2283, 2010.

[8] M. Shin, "NEGF Simulation of Nanowire Field Effect Transistors Using the Eight-band k.p method," in Computational Electronics, 2009. IWCE '09. 13th International Workshop on, 2009.

[9] S. Datta, "Quantum Transport: Atom to Transistor", Cambridge University Press (ISBN-13: 9780521631457, ISBN-10: 0521631459.

[10] J. M. Hinckley, and J. Singh, "Influence of substrate composition and crystallographic orientation on the band structure of pseudomorphic Si-Ge alloy films," Physical Review B, vol. 42, no. 6, pp. 3546-3566, 1990..

[11] Pham, A.T., Jungemann, C., Meinerzhagen, B.: Microscopic modeling of hole inversion layer mobility in unstrained and uniaxially stressed Si on arbitrarily oriented substrates. Solid State Electron. 52, 1437–1442 (2008)

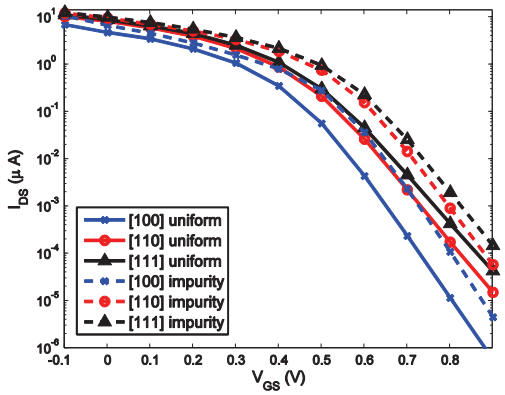

Fig. 4. I_{DS}-V_{GS} characteristic for different crystal orientations in the presence of impurity atom. The on-current is almost unchanged due to weal influence of impurity.

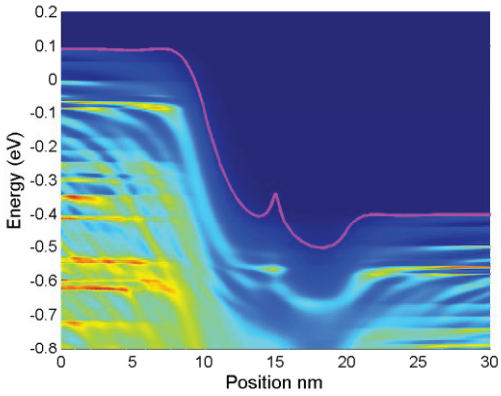

Fig. 7. Energy-resolved density of state (LDOS) at V_{GS}=0.5 V for nanowire in [100] direction. Impurity induced resonance levels are situated at lower subbands.

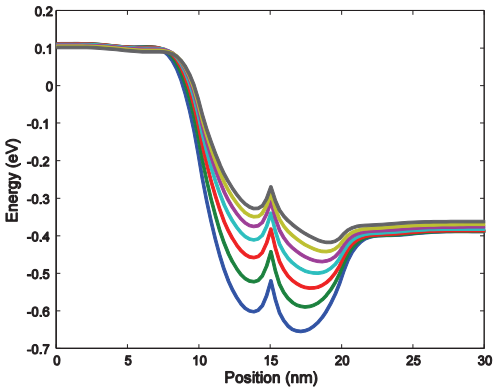

Fig. 5. First subband energy profile for different values of V_{GS}. At high V_{GS} values the influence of impurity becomes weaker.

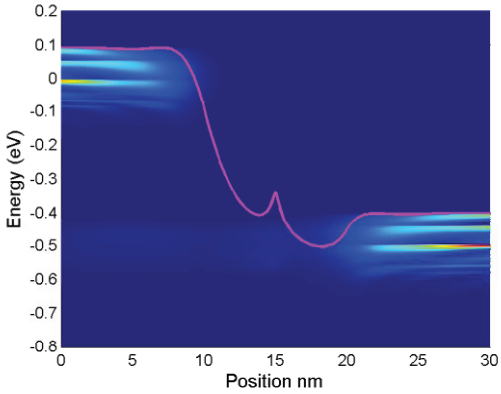

Fig. 8. Energy-resolved charge density $G_n(x,E)$ at V_{GS}=0.5 V for nanowire in [100] direction.

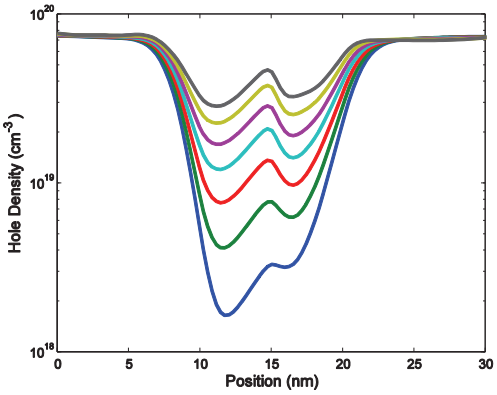

Fig. 6. 1D hole density in [100] nanowire.

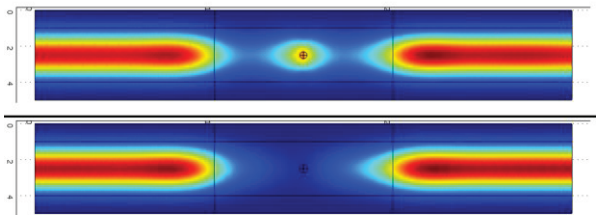

Figure 9. 2D hole density at V_{GS}=0.9 V and V_{GS}=0.3 V.